

28 GHz Wireless Channel Characterization for a Quantum Computer Cryostat at 4 Kelvin

Ama Bandara*, Viviana Centritto Arrojo*, Heqi Deng†, Masoud Babaie†, Fabio Sebastiani†, Edoardo Charbon†, Evgenii Vinogradov*, Eduard Alarcón*, Sergi Abadal*

*Nanonetworking Center in Catalunya, Universitat Politècnica de Catalunya, Barcelona, Spain

† Delft University of Technology, 2628 CD Delft, The Netherlands

‡ Ecole Polytechnique Fédérale de Lausanne (EPFL), Switzerland

*ama.peramuna@upc.edu

Abstract—The scalability of quantum computing systems is constrained by the wiring complexity and thermal load introduced by dense wiring for control, readout and synchronization at cryogenic temperatures. To address this challenge, we explore the feasibility of wireless communication within a cryostat for a multi-core quantum computer, focusing on wireless channel characterization at cryogenic temperatures. We propose to place on-chip differential dipole antennas within the cryostat, designed to operate at 28 GHz in temperatures as low as 4 K. We model the antennas inside a realistic cryostat and, using full-wave electromagnetic simulations, we analyze impedance matching, spatial field distribution, and energy reverberation due to metallic structures. The wireless channel is characterized through measured channel impulse response (CIR) across multiple receiver antenna positions. The results demonstrate potential for reliable short-range communication with high Signal-to-Noise Ratio (SNR) and limited sensitivity to positional variation, at the cost of non-negligible delay spread, due to significant multipath effects.

I. INTRODUCTION

The fast-evolving landscape of quantum computing requires practical solutions to move beyond the Noisy Intermediate-Scale Quantum (NISQ) era [1]. Achieving quantum advantage for classically intractable problems demands systems with millions of qubits [2]. However, scalability is constrained, among other aspects, by the vertical interconnects linking cryogenic quantum processors and room-temperature control electronics [3]. These dense wire bundles introduce spatial congestion and thermal load which degrades qubit coherence.

One approach to alleviate the vertical wiring bottleneck is to integrate control and readout circuits closer to the qubits. In this regard, advances in cryo-CMOS electronics [4], [5] enable local control, readout, and synchronization at 4 K. This approach is complementary to the recent emergence of modular quantum architectures [6]–[9] which address scalability by interconnecting multiple Quantum Processing Units (QPUs) horizontally at cryogenic temperatures.

The convergence of modular quantum architectures with the local control circuit approach, albeit promising, poses new interconnect requirements. This is because the control and readout circuits of each QPU shall be interconnected to

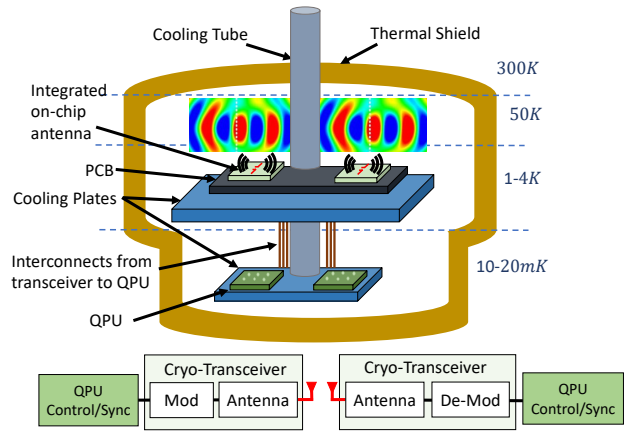


Fig. 1: Integrated on-chip differential dipole antennas inside the cryostat, which are positioned above the QPUs. The cryo-transceivers are connected to the QPUs through wires, while the wireless plane is fulfilling the need for classical interconnects (control/synchronization) in a modular architecture.

synchronize operation and orchestrate quantum state transfers across the QPUs, possibly across multiple dies or even boards. This communication can be performed through wired interconnects, yet it could be slow and inefficient if the signaling needs to propagate across multiple boards.

To further enhance scalability, complementing wired horizontal interconnects with wireless links (Fig. 1) offers global reconfigurability and low latency while operating with minimal thermal impact [10]. Furthermore, due to the minimal thermal noise at cryo-CMOS RF-transceivers, the Signal-to-Noise Ratio (SNR) of such communication is expected to be high, even for very low transmission powers.

Implementing wireless links within a cryostat introduces new electromagnetic challenges. The quantum computer is physically enclosed within a cryostat chamber, which contains power cables, metallic plates for separate cooling stages, metallic cooling tubes, heat shielding materials as the enclosure, and other solid structures with varying material properties. These components create a reverberant environment with multipath propagation that can perturb nearby qubits. Such an enclosed environment resembles the chip-scale wireless

Authors gratefully acknowledge funding from the European Commission via projects with GA 101042080 (WINC) and 101099697 (QUADRATURE).

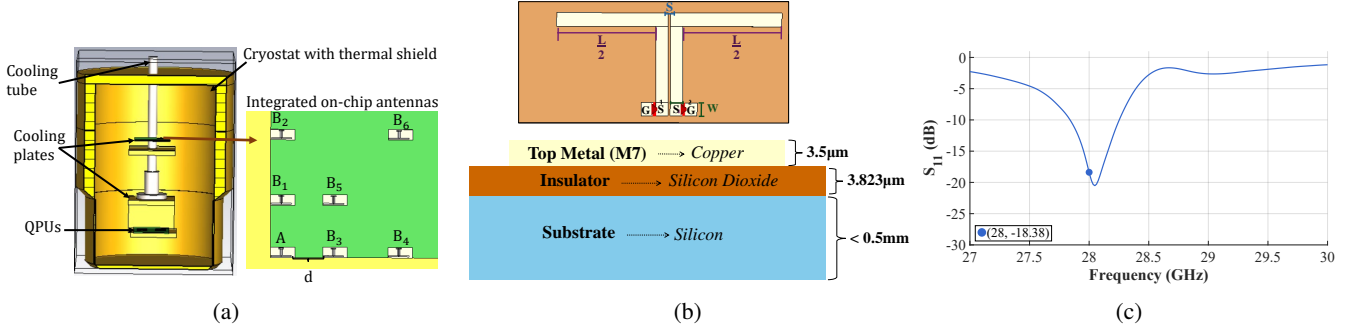


Fig. 2: Simulation setup implemented in CST MWS. (a) Cross-section of the simulation model of the cryostat, together with a detailed map of the evaluated antenna positions within the boundaries of 4 K temperature level. (b) Top-view and cross-section of the differential-fed dipole antenna design, including details on the thickness of the top metal, insulator and substrate layer. (c) Reflection coefficient (dB) of the on-chip differential dipole within the cryostat, showing operation at 28 GHz.

communication approach, the channel characterization aspects of which have been surveyed in [11] from mmWave to optical frequencies. Moreover, prior research has explored various on-chip antenna designs [12]–[14], [14]–[18]. However, the design and characterization of on-chip antennas for cryo-CMOS environments remain largely unexplored.

In recent literature, cryo-wireless interconnects have been gaining interest. In [19], wireless signal transmission using a wideband 8–12 GHz patch antenna inside a dilution refrigerator was investigated, but only assessed at 77 K. In [20], a wireless vertical communication system between 4 K and 300 K at 260 GHz has been explored. The system consisted of a horn antenna positioned at the high temperature level, pointing towards the lower part of the cryostat, where a set of on-chip antennas at 4 K would backscatter readout signals. The on-chip antennas showed improved efficiency from 38% at 300 K to 67%–97% due to the considerable improvement of copper’s electrical conductivity. However, to the best of our knowledge, an analysis for horizontal links inside a quantum computer cryostat at 4 K temperature does not exist.

To bridge this gap, we implement a realistic cryostat model [21] in CST Microwave Studio [22] with the main goal of characterizing the wireless channel for horizontal communication across QPUs. Following frequency planning guidelines, we design a 28 GHz on-chip differential dipole antenna separated from the spin-qubit operation band at 16 GHz [23]. The antenna is optimized for operation at 4 K and compatible with cryo-CMOS transceivers. As main contribution, we then characterize the resulting wireless channel inside the cryostat to evaluate its feasibility, considering the effects of enclosure geometry and material properties at cryogenic temperatures. To this end, we measure the channel impulse response (CIR), from which we infer signal strength, delay spread, and SNR at cryogenic conditions.

The rest of the paper is organized as follows. Section II describes the design and placement of the on-chip differential dipole antenna, the cryostat characteristics, and metrics of study. In Section III, we present the antenna and channel characterization results. Finally, Section IV summarizes the key contributions and outlines directions for future research.

II. METHODOLOGY

In this section, we provide a detailed description of the (i) design of the differential dipole antenna in cryogenic temperature, (ii) integration of the proposed antenna design into the cryostat, (iii) the channel characterization and performance metrics used for evaluation.

A. Cryo-CMOS Antenna Model

The proposed antenna is a differential dipole integrated in cryo-CMOS technology [4], [5], designed to operate at 28 GHz within the cryostat. The choice of differential dipole antenna is based on its noise immunity and ability to suppress common-mode interference through differential feeding [24]. The choice of the frequency is backed up by the relatively small wavelength, ease of on-chip integration, the maturity of designs for 5G applications, and sufficient distance to resonance frequency of spin-qubits [23]. Full details of the design are given in [25].

The dipole, illustrated in Fig. 2b, comprises two co-linear copper arms deposited on a Silicon Dioxide (SiO_2) layer, where the initial resonant length L can be estimated as $L = \frac{\lambda_0}{2\sqrt{\epsilon_{eff}}}$, where λ_0 denotes the free-space wavelength and $\epsilon_{eff} = \frac{\epsilon_r + 1}{2}$ represents the effective permittivity of the antenna, with ϵ_r being the permittivity of the substrate. The final optimal dimensions were refined through iterative adjustments of the length of the dipole’s arms.

The antenna is fed through a differential feeding network consisting of two coplanar microstrip lines (MLSSs) located on the SiO_2 layer. The width (W) and spacing (S) of the lines were calculated based on the substrate properties and dimensions. Finally, the MLSSs terminate in a ground-signal-signal-ground (GSSG) pad configuration.

The proposed on-chip antenna is embedded in a CMOS layered stack, as shown in Fig. 2b. The copper dipole is positioned on the top metal layer, M7, beneath which lies a thick SiO_2 layer serving as an insulating medium, followed by a bottom Si substrate [26]. The antenna design incorporates the Cu conductivity, Si conductivity, Si permittivity, and SiO_2 permittivity as $2.9 \times 10^8 \text{ S/m}$, $4.26 \times 10^{-7} \text{ S/m}$, 11.45 and 3.9

respectively, at cryogenic temperature [27], [28]. These values differ from the properties at room temperature and affect the antenna performance as detailed in [25].

B. Cryostat Model

The cryostat, outlined in Fig. 2a, is a cylindrical enclosure which is used to isolate the quantum computer from the external noise and interference, while maintaining the adequate thermal profile. The outer layer of the cryostat is consisting of shielding material for magnetic interference and inner layer is with a thermal shield. Based on the refrigeration system used to maintain the temperature, there are different temperature levels at each stage of the cryostat that reach 10-20 mK at the bottom, where the QPUs are housed. In addition to the wired interconnects, each temperature stage contains cooling plates, cooling tubes, and other metallic components, which contribute to multipath signal reflections and signal attenuation due to their material properties and geometric obstructions.

The proposed differential dipole antennas are placed at the 4 K temperature together with the cryo-CMOS control circuits [25], located above the QPUs. The in-plane separation distance between the different antennas varies from 0.75λ to 2.6λ as shown in Fig. 2a. Vertically, there are three cooling plates connected to the central cooling tube, where two plates resemble a stage to house the QPUs and one plate is placed above the mK temperature level. The thermal shield exhibits reflective properties for the electromagnetic waves which is made of metallic alloys [21]. This placement helps to reduce communication latency while minimizing thermal interference caused by RF radiation. The size of the cryostat is 30 cm diameter with 70 cm height, with the top-middle and middle-bottom plate separation being 15 cm and 10 cm, respectively, based on the range of standard cryostat dimensions used for quantum computing applications, e.g., in [21]. The antenna plane is on top of the top plate.

C. Performance Metrics

Next, we analyze the performance metrics which we used for the channel characterization. We consider a single transmitter (TX) antenna A and multiple receiver (RX) antennas B_1 - B_6 , one level above the QPUs as shown in Fig. 2a. Using the full-wave time-domain solver of CST, we excite the TX with an impulse and record the resulting CIR, denoted as $h(t)$, at the RX antennas. The wireless links are evaluated for each pair of TX-RX antennas that result in different separation distances and alignments along the two directions in the chip plane, relative to the fixed position of the TX antenna A .

1) *Signal to Noise Ratio*: To quantify the amount of energy received at RX with extensive multipath propagation in the enclosed cryostat environment, we assume a unitary transmitted energy. Then, we measure the SNR of the wireless link as

$$SNR = \frac{P_{TX} \int |h(\tau)|^2 d\tau}{N}, \quad (1)$$

this is, dividing the total received signal strength of the message sent with a transmit power of P_{TX} , integrated over the entire time period, by the noise power N .

The power of the thermal noise is characterized by, $K_B T B$ where K_B is the Boltzmann's constant, T is the temperature in Kelvin and B is the finite bandwidth of the system. However, this formula is an approximation for low frequencies and room temperatures of the more general Nyquist equation [29]

$$N = \frac{h f_c B}{\exp(\frac{h f_c}{K T}) - 1}, \quad (2)$$

where f_c is the operating frequency of the antenna and h is Planck's constant.

2) *Delay Spread*: Using the dispersive wireless channel response $h(t)$, we evaluate the root mean square (RMS) delay spread as a measure of the multipath effects, as given by:

$$DS_{RMS} = \sqrt{\frac{\int |h(\tau)|^2 (\tau - \bar{\tau})^2 d\tau}{\int |h(\tau)|^2}}, \quad (3)$$

where the mean delay is $\bar{\tau} = \frac{\int |h(\tau)|^2 \tau d\tau}{\int |h(\tau)|^2}$.

III. PERFORMANCE EVALUATION

To characterize the wireless channel using differential dipole antennas in a cryostat environment, we implement the cryostat model and antennas in CST Microwave Studio [22] using the directives of the previous section.

A. On-Chip Antenna Inside the Cryostat

The integrated on-chip antenna inside the cryostat is simulated using two discrete ports placed on GSSG pads, excited by impulse signals. The antenna design is fine-tuned to achieve efficient radiation and proper impedance matching to the cryostat environment. The optimized dipole length has been determined to be $L_{opt} = 3.06$ mm. As shown in Fig. 2c, the reflection coefficient of the transmitter antenna S_{11} exhibits a resonance close to 28 GHz with a minimum value of -21 dB, indicating a proper impedance matching and enhanced radiation performance within the cryostat.

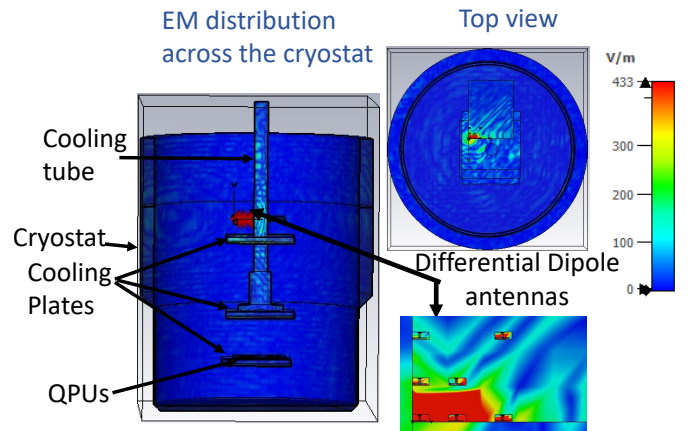


Fig. 3: Spatial distribution of the electrical field across the cryostat as observed in the cross-section, general top view, and top view at the plane of the antennas.

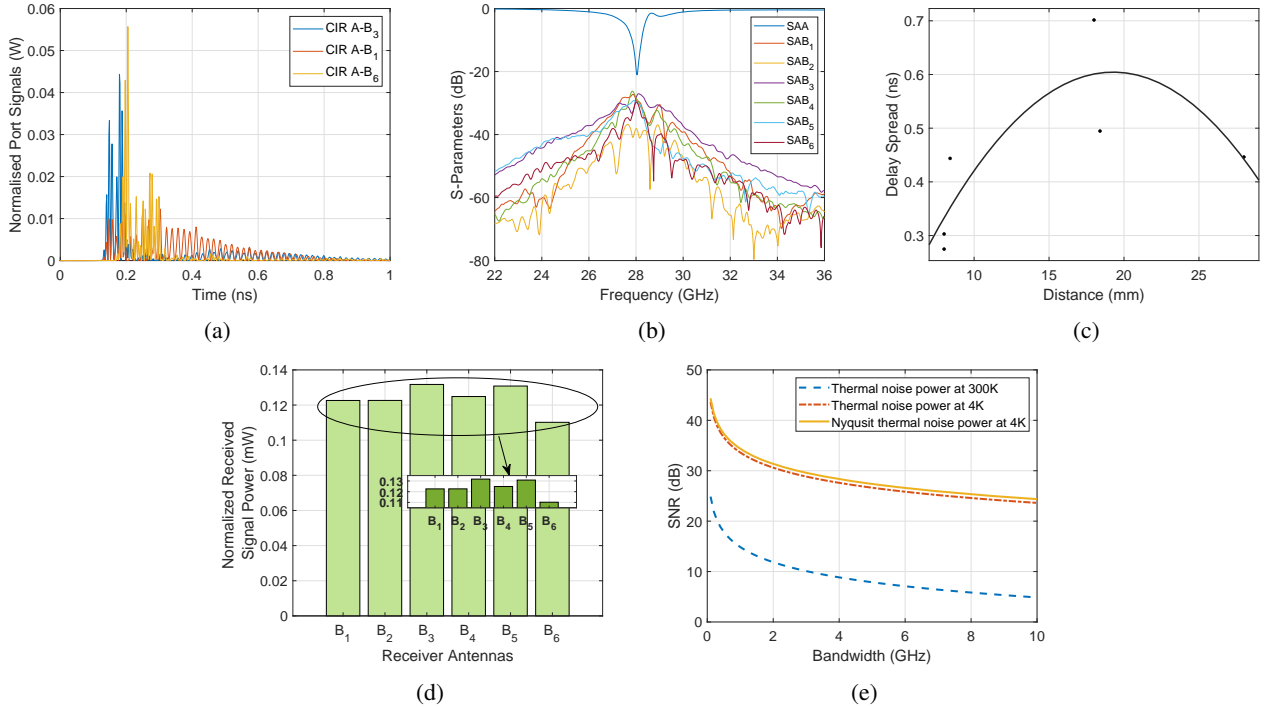


Fig. 4: Characterization of the wireless channel in a 4-K cryostat environment at 28 GHz. (a) Measured power delay profile of the wireless links $A - B_1$, $A - B_3$, $A - B_6$ with $P_{TX} = 0$ dB (b) Return loss of transmitter A and S_{21} of the different antenna for B_1 , B_3 , B_6 . (c) Delay spread over distance for the wireless links $A - B_{1-6}$ with differential feeds. (d) Received power at intended antenna positions of B_{1-6} from a single transmission. (e) SNR as a function of bandwidth assuming $P_{TX} = -30$ dBm.

The spatial field distribution of the antenna is observed in Fig. 3. The antennas are placed 6 cm above the second cooling plate to minimize the effects of the structure. The figure shows how the energy is distributed primarily through the PCB that holds the antennas, within its same temperature level. Due to reflections and scattering effects, the signal energy also travels to other temperature levels, with some radiation arriving to the cooling plate below. Significant amount of radiation arrives to the antennas that are co-lateral, either because the differential feed radiates or because of common substrate effects or reflections from the tubes or enclosure present in the environment.

B. Wireless Channel

Multipath effects are observed in the measured CIR as shown in Fig. 4a, corresponding to the links $A - B_3$, $A - B_6$, $A - B_1$. These effects are due to the enclosed nature of the cryostat and the radiation impairments introduced by the silicon substrate of the on-chip antenna, which result in different delay profiles. Fig. 4b shows the reflection and transmission coefficients (S-parameters) of the channels. Most links show a similar value of the transmission coefficient at 28 GHz, which underscores the influence of reflections and other phenomena reducing the impact of distance on the link response.

In Fig. 4c, the RMS delay spread of the CIR is obtained as detailed in prior sections. It is observed that the delay spread is relatively high, between 0.3 and 0.7 ns, leading to

coherence bandwidths $B \sim DS^{-1}$ of a few GHz at most. The delay spread initially increases with distance, indicating that the main *direct ray* for communication weakens while distant reflections gain importance. At higher distances, the delay spread is slightly reduced as all reflections seem to be equally important. This is a usual behavior in enclosed environments [11].

The received power at each antenna position from B_1 to B_6 is shown in Fig. 4d, illustrating how much energy is radiated towards each receiver antenna. Such localized power concentrations could potentially affect neighboring QPUs if the radiated power exceeds the allowable thermal dissipation threshold within the cryostat. Even though the separation between antennas ranges between 0.75λ and 2.6λ depending on the receiver antenna position, the received power remains largely independent of the distance, showing only minor variations. This is mainly due to energy reverberation within the cryostat. The tradeoff, then, lies in the energy-delay correlation since, owing to this reverberant behavior, both high energy and delay spread can be expected.

In Fig. 4e, the SNR is measured as detailed in prior sections, and represented for varying bandwidths and different thermal noise power models at a transmit power of -30 dBm. The thermal noise added at the receiver is inherently low at high frequencies and cryogenic temperatures due to low carrier mobility at low temperatures. Yet, when the bandwidth increases, the noise is proportionally increasing, thereby reducing the

SNR. Furthermore, it is observed that there is a significant increase of SNR in 4 K compared with room temperature due to low noise figures.

IV. CONCLUSION

In this paper, we have analyzed the feasibility of wireless communication inside a cryostat through integration of on-chip differential dipole antenna operating at 28 GHz down to 4 K. Through full wave simulations, the proposed antenna demonstrated efficient radiation with good impedance matching ($S_{11} \approx -21$ dB) in a cryogenic environment. Channel characterizations have shown that even with energy reverberation and multipath effects, the wireless links maintain a high SNR with low noise. Moreover, the received power at each antenna location is similar, revealing that the spatial energy is dispersed and an adequate received power is obtained despite the distance for wireless receivers. In the near future, we plan to explore the behavior of transmissions under different antenna design strategies and analyze the classical-quantum interconnects while assessing their error rates and interference characteristics, so as to enhance scalability and reliability in multi-core quantum systems. Further, we also aim to assess the amount of radiation that may impact on the QPUs and hence interfere with the qubit operation, to then develop protection measures.

REFERENCES

- [1] J. Preskill, "Quantum computing in the NISQ era and beyond," *Quantum*, vol. 2, p. 79, 2018.
- [2] T. D. Ladd, F. Jelezko, R. Laflamme, Y. Nakamura, C. R. Monroe, and J. L. O'Brien, "Quantum computers," *Nature*, vol. 464, pp. 45–53, 2010.
- [3] A. Das, M. Palesi, J. Kim, and P. P. Pande, "Chip and package-scale interconnects for general-purpose, domain-specific and quantum computing systems—overview, challenges and opportunities," *IEEE Journal on Emerging and Selected Topics in Circuits and Systems*, 2024.
- [4] E. Charbon, M. Babaie, A. Vladimirescu, and F. Sebastianiano, "Cryogenic CMOS Circuits and Systems: Challenges and Opportunities in Designing the Electronic Interface for Quantum Processors," *IEEE Microwave Magazine*, vol. 22, no. 1, pp. 60–78, 2021.
- [5] B. Patra, R. M. Incandela, J. P. G. van Dijk, H. A. R. Homulle, L. Song, M. Shahmohammadi, R. B. Staszewski, A. Vladimirescu, M. Babaie, F. Sebastianiano, and E. Charbon, "Cryo-CMOS circuits and systems for quantum computing applications," *IEEE Journal of Solid-State Circuits*, vol. 53, no. 1, pp. 309–321, 2018.
- [6] K. R. Brown, J. Kim, and C. Monroe, "Co-designing a scalable quantum computer with trapped atomic ions," *npj Quantum Information*, vol. 2, no. 1, p. 16034, 2016. [Online]. Available: <https://doi.org/10.1038/npjqi.2016.34>
- [7] N. Isailovic, Y. Patel, M. Whitney, and J. Kubiatowicz, "Interconnection networks for scalable quantum computers," in *33rd International Symposium on Computer Architecture (ISCA'06)*, 2006, pp. 366–377.
- [8] C. Monroe, R. Raussendorf, A. Ruthven, K. R. Brown, P. Maunz, L.-M. Duan, and J. Kim, "Large-scale modular quantum-computer architecture with atomic memory and photonic interconnects," *Physical Review A*, vol. 89, no. 2, p. 022317, 2014.
- [9] E. Alarcón, S. Abadal, F. Sebastianiano, M. Babaie, E. Charbon, P. H. Bolívar, M. Palesi, E. Blokhina, D. Leipold, B. Staszewski, A. García-Sáez, and C. G. Almudever, "Scalable multi-chip quantum architectures enabled by cryogenic hybrid wireless/quantum-coherent network-in-package," in *2023 IEEE International Symposium on Circuits and Systems (ISCAS)*, 2023.
- [10] P. Escofet, S. B. Rached, S. Rodrigo, C. G. Almudever, E. Alarcón, and S. Abadal, "Interconnect fabrics for multi-core quantum processors: A context analysis," in *Proceedings of the 16th International Workshop on Network on Chip Architectures*, 2023, pp. 34–39.
- [11] S. Abadal, C. Han, and J. M. Jornet, "Wave propagation and channel modeling in chip-scale wireless communications: A survey from millimeter-wave to terahertz and optics," *IEEE Access*, vol. 8, pp. 278–293, 2020.
- [12] W. Rayess *et al.*, "Antennas and Channel Characteristics for Wireless Networks on Chips," *Wireless Personal Communications*, vol. 95, no. 4, pp. 5039–5056, 2017.
- [13] G. Bellanca, *et al.*, "Integrated vivaldi plasmonic antenna for wireless on-chip optical communications," *Optics express*, vol. 25, no. 14, 2017.
- [14] X. Timoneda, A. Cabellos-Aparicio, D. Manessis, E. Alarcón, and S. Abadal, "Channel characterization for chip-scale wireless communications within computing packages," in *2018 Twelfth IEEE/ACM International Symposium on Networks-on-Chip (NOCS)*, 2018.
- [15] V. Pano, I. Tekin, I. Yilmaz, Y. Liu, K. R. Dandekar, and B. Taskin, "TSV antennas for multi-band wireless communication," *IEEE Journal on Emerging and Selected Topics in Circuits and Systems*, vol. 10, no. 1, pp. 100–113, 2020.
- [16] F. Gutierrez, S. Agarwal, K. Parrish, and T. S. Rappaport, "On-chip integrated antenna structures in CMOS for 60 GHz WPAN systems," *IEEE Journal on Selected Areas in Communications*, vol. 27, no. 8, pp. 1367–1378, 2009.
- [17] S. Pan and F. Capolino, "Design of a CMOS On-Chip Slot Antenna With Extremely Flat Cavity at 140 GHz," *IEEE Antennas and Wireless Propagation Letters*, vol. 10, pp. 827–830, 2011.
- [18] J. W. May, R. A. Alhalabi, and G. M. Rebeiz, "A 3 G-Bit/s W-band SiGe ASK receiver with a high-efficiency on-chip electromagnetically-coupled antenna," in *2010 IEEE Radio Frequency Integrated Circuits Symposium*, 2010, pp. 87–90.
- [19] J. u. Rehman Kazim, M. Z. Ali, A. Al-Moathin *et al.*, "Wireless microwave signal transmission for cryogenic applications," in *2023 IEEE International Symposium on Antennas and Propagation and USNC-USRI Radio Science Meeting (USNC-USRI)*, 2023, pp. 43–44.
- [20] J. Wang, I. Harris, M. Ibrahim, D. Englund, and R. Han, "A wireless terahertz cryogenic interconnect that minimizes heat-to-information transfer," *Nature Electronics*, vol. 8, no. 5, pp. 426–436, 2025.
- [21] "Cryogenic measurement systems for quantum technology," <https://bluefors.com/applications/quantum-technology/>, Bluefors, 2025, accessed: 2025-10-09.
- [22] "CST Microwave Studio," 2022. [Online]. Available: <http://www.cst.com>
- [23] S. G. J. Philips, M. T. Madzik, S. V. Amitonov, S. L. de Snoo, M. Russ, N. Kalhor, C. Volk, W. I. L. Lawrie, D. Brousse, L. Tryputen, B. Paquet-let Wüetz, A. Sammak, M. Veldhorst, G. Scappucci, and L. M. K. Vandersypen, "Universal control of a six-qubit quantum processor in silicon," *Nature*, vol. 609, pp. 919–924, 2022.
- [24] A. Shamim, L. Roy, N. Fong, and N. G. Tarr, "24 GHz on-chip antennas and baluns on bulk si for air transmission," *IEEE Transactions on Antennas and Propagation*, vol. 56, no. 2, pp. 303–311, 2008.
- [25] V. Centritto, A. Bandara, H. Deng, M. Babaie, E. Vinogradov, S. Abadal, and E. Alarcon, "Cryo-CMOS antenna for wireless communications within a quantum computer cryostat," *arXiv preprint arXiv:2510.13627*, 2025.
- [26] H. M. Cheema and A. Shamim, "The last barrier: on-chip antennas," *IEEE Microwave Magazine*, vol. 14, no. 1, pp. 79–91, 2013.
- [27] B. Patra, M. Mohammadreza, A. Ruffino, F. Sebastianiano, E. Charbon, and M. Babaie, "Characterization and analysis of on-chip microwave passive components at cryogenic temperatures," *Electronics Devices Society*, vol. 8, pp. 448–456, 2020.
- [28] J. Krupka, J. Breeze, A. Centeno, N. Alford, T. Claussen, and L. Jensen, "Measurements of permittivity, dielectric loss tangent, and resistivity of float-zone silicon at microwave frequencies," *IEEE Transactions on Microwave Theory and Techniques*, vol. 54, no. 11, pp. 3995–4001, 2006.
- [29] H. Nyquist, "Thermal agitation of electric charge in conductors," *Phys. Rev.*, vol. 32, pp. 110–113, Jul 1928.